Available online at www.sciencedirect.com
ScienceDirect
Journal of Photochemistry and Photobiology A: Chemistry 186 (2007) 8–13
Journal of Photochemistry and Photobiology A:Chemistry
www.elsevier.com/locate/jphotochem

Investigation of photocatalytically-active hydrated forms of amorphous titania, $TiO_2 \cdot nH_2O$

Zhenyu Zhang, Paul A. Maggard *

Department of Chemistry, 2620 Yarbrough Drive, North Carolina State University, Raleigh, NC 27695-8204, USA

Received 2 May 2006; received in revised form 3 July 2006; accepted 5 July 2006
Available online 13 July 2006

Abstract

Low temperature preparations of hydrated forms of amorphous titania, $TiO_2 \cdot nH_2O$, have been obtained starting from Ti(*n*-butoxide)$_4$ in ethanol, acetone, hexane or tetrahydrofuran solutions by either slow evaporation (TiO_2–A1) or from rapid precipitation in an aqueous HCl solution using ammonia (TiO_2–A2). The washed products lost/reabsorbed water up to a maximum of 19 wt.% for samples of TiO_2–A1 ($n \sim 1.0$) and 9.9% for TiO_2–A2 ($n \sim 0.5$), determined from TGA, and exhibited an optical band gap of ~3.5 eV. Under full spectrum irradiation in aqueous methanol solutions the photocatalytic rates for H_2 production reached a maximum of 314 and 1158 $\mu mol\, h^{-1}\, g^{-1}$ for bare and platinized (0.5 wt.%) samples of TiO_2–A1, respectively, and 210 and 170 $\mu mol\, h^{-1}\, g^{-1}$ for TiO_2–A2. The photocatalytic rates measured at a slightly elevated temperature of 58 °C were up to 2× greater than those measured nearer room temperature, while these rates were independent of the amount or type of solvent used in their preparation. The UV–vis diffuse reflectances, post irradiation, indicate a higher concentration of Ti^{3+} sites in TiO_2–A1 compared to TiO_2–A2, and thus a higher density of active sites and reduced electron–hole recombination.

Keywords: Amorphous titania; Photocatalysis

1. Introduction

Photocatalytic reactions over metal-oxide surfaces have been extensively investigated over the last two decades and have been motivated by applications focusing on the production of useful chemical fuels (e.g. H_2, CH_4, NH_3) from solar energy and abundantly available feedstocks (H_2O, CO_2, N_2) [1]. Some of the most intensely investigated metal oxides include TiO_2 [2], ZrO_2 [3], Ta_2O_5 [4], $SrTiO_3$ [5], $NaTaO_3$ [6], and WO_3 [7], and which are photostable and photocatalytically active for a wide range of redox reactions initiated by band-gap illumination. In TiO_2, for example, the photocatalytic efficiency can be increased with increasing surface area, the loading of a surface cocatalyst such as Pt (for H_2 evolution) or RuO_2 (for O_2 evolution), the addition of sacrificial reductants (CH_3OH), and by preparation of the crystalline anatase form [1,2,8–12]. The highest rates are known for nanocrystalline anatase co-loaded with Pt/RuO_2. Nano-sized crystal grains of TiO_2 have larger band gap sizes and higher conduction band levels to accomplish the reduction of H_2O to H_2, while the conduction band level is unfavorably lower in both rutile and larger-grained anatase forms. By comparison, amorphous TiO_2 has a band gap equal to or greater than nanocrystalline anatase, and therefore may have a conduction band level suitable for the efficient photocatalytic reduction of H_2O.

However, nearly all photocatalytic studies on TiO_2 have focused on its crystalline forms, as it is commonly accepted that amorphous metal oxides contain high concentrations of defects that will invariably function as rapid electron–hole recombination centers to render them inactive [13–15]. Thus, investigations based on the synthesis and photocatalytic activity of amorphous TiO_2 are relatively few [13–15], and based mostly on commercially available and non-hydrated forms that are reported as having negligible activity alongside a more complete study of the crystalline anatase form. However, hydrated forms of metal oxides, such as found in layered perovskites, often exhibit markedly higher activities [16,17]. Despite intense research efforts, there are no studies (to our knowledge) concerning the synthetic preparations of hydrated and amorphous forms of TiO_2 with significant photocatalytic

* Corresponding author. Tel.: +1 919 515 3616; fax: +1 919 515 5079.
E-mail address: Paul_Maggard@ncsu.edu (P.A. Maggard).

1010-6030/$ – see front matter © 2006 Elsevier B.V. All rights reserved.
doi:10.1016/j.jphotochem.2006.07.004

rates for H_2 evolution. In contrast, amorphous forms of ZrO_2 and Nb_2O_5 have recently been shown to exhibit photocatalytic rates that are higher than their crystalline counterparts, such as measured in aqueous methanol [18,19]. Other potential advantages of hydrated forms of amorphous metal oxides are that they can be prepared at room temperatures, are easier to process into different shapes and forms, exhibit high surface areas, and allow for a wider range of chemical species to be doped/imbedded into their matrix compared to crystalline forms [20].

Described herein is the preparation and investigation of hydrated forms of amorphous TiO_2 that exhibit significant photocatalytic activity for H_2 evolution in aqueous methanol solutions. The products were characterized using thermogravimetric analysis, FT-IR, powder X-ray diffraction, SEM, and UV–vis diffuse reflectance. The photocatalytic rates were measured and analyzed with respect to the amount Pt surface cocatalyst (0–5%), for different solvents used in the syntheses, and for the dependence on elevated reaction temperatures.

2. Experimental: synthesis

Amorphous and hydrated TiO_2 was prepared by dissolving a weighed amount of Titanium (IV) *n*-butoxide (2 g, 0.00588 mol; Alfa Aesar, 99+%) into either pure ethanol (2, 5, 10, or 20 ml), acetone (5 ml), hexane (5 ml), or tetrahydrofuran (5 ml). Each of these solutions was mixed for 10 min and aged at room temperature for 24–48 h, during which time all of the solvent had evaporated and an amorphous white powder was obtained. To remove the remaining organic species, each powder was re-dispersed in 20 ml of deionized water (1:100 solid/water ratio) and dried at 80 °C for 1 h to yield amorphous $TiO_2{\cdot}nH_2O$ powders labeled the TiO_2-A1 series. Another preparation of amorphous TiO_2 was performed by dissolving the Titanium (IV) *n*-butoxide into 3 ml of concentrated HCl, followed by the dropwise addition of concentrated aqueous ammonia with vigorous stirring until the pH of the solution reached 14. The obtained precipitate was filtered and washed in water repeatedly until no traces of AgCl precipitate occurred upon addition of 0.5 M $AgNO_3$. The sample washing is critical to remove surface Cl^- ions, which can suppress photocatalytic activity [1,21]. This product was dried at 80 °C and labeled TiO_2–A2.

3. Characterization techniques

High-resolution powder X-ray diffraction (PXRD) of the products was collected on an INEL diffractometer using Cu $K\alpha_1$ ($\lambda = 1.54056$Å) radiation from a sealed tube X-ray generator (35 kV, 30 mA) in transmission mode and using a curved position sensitive detector (CPS120). Scanning electron microscopy (SEM) was performed on a JEOL JEM 6300 in order to examine the particle morphologies and sizes. Thermogravimetric analyses of the amorphous products were taken on a TA Instruments TGA Q50, where each sample was loaded onto a Pt pan, equilibrated and tarred at room temperature, and heated at a rate of 5 °C/min to 900 °C under flowing nitrogen. The UV–vis diffuse reflectance of each sample was measured on a Cary 300 spectrophotometer equipped with an integrating sphere, wherein approximately 50 mg of each sample was mounted onto a fused-silica holder and placed along the external window of the integrating sphere. Pressed polytetrafluoroethylene powder was used as a reference and the data were plotted as the remission function $F(R_\infty) = (1 - R_\infty)^2/(2R_\infty)$, where R is diffuse reflectance based on the Kubelka-Monk theory of diffuse reflectance. Mid-infrared (400–4000 cm^{-1}) spectra were collected on a Mattson Genesis II FTIR spectrometer operating at a resolution of 2 cm^{-1}. Each sample was ground and pelletized with dried KBr, transferred to the FTIR, and evacuated for 2–5 min before spectra acquisition.

4. Photocatalytic measurements

The photocatalytic rates were tested according to previously published procedures [10,22]. A weighed amount of each sample (~100 mg) was transferred to a ~30 ml cylindrical vessel made of fused silica with a magnetic stir bar at the bottom, and which was then connected at the top to a smaller 4 mm(i.d.) × 50 mm length tube. The samples were loaded with Platinum (0.1, 0.5, 1.0 or 5.0 wt.%) cocatalyst by the photodeposition method, where Pt is a well-known aid in the surface reduction of H_2O to give H_2: ~50 mg of amorphous $TiO_2{\cdot}nH_2O$ was suspended via stirring in 20 mL of an aqueous solution of dihydrogen hexachloroplatinate(IV) ($H_2PtCl_6{\cdot}6H_2O$; Alfa Aesar, 99.95%) inside a fused silica tube that was then irradiated for 2 h using a 400 W Xe arc lamp. After platinization, the solid was filtered and allowed to dry at room temperature and was then resuspended inside the fused-silica tube in 50 ml of a 20% aqueous methanol solution. This was stirred continuously under irradiation with full solar spectrum light (200 to >1000 nm) using a 400 W Xe arc lamp, and using a high speed fan and/or an ice bath to control container temperature. During the course of the photocatalytic reactions the generated gas bubbles appeared to attach to the TiO_2 particles and rose to the top of the tubing. The rate of the photocatalytic reaction was measured volumetrically using a horizontal tube that was attached to the top of the reaction vessel and contained a mobile liquid plug. The change in the position of the liquid plug was monitored hourly and used to calculate the amount of gases generated. Identity of the formed gases and their molar ratios were characterized via injection into a GC (SRI MG #2, helium ionization and thermal conductivity detectors). Selected GC data are available in the Supplementary Information. Photocatalytic measurements for each sample were typically continued over the course of a full day, and for several samples the photocatalytic rates were tested over a 3–8 day period.

5. Results and discussion

5.1. Synthesis and physical characterization

Two different types of synthetic preparations of amorphous hydrated $TiO_2{\cdot}nH_2O$ were investigated, using either a slow evaporation of a solvent containing Ti(*n*-butoxide)$_4$ (TiO_2–A1 series) or its rapid precipitation from a concentrated HCl solution (TiO_2–A2). Discussion of the TiO_2–A1 series will focus

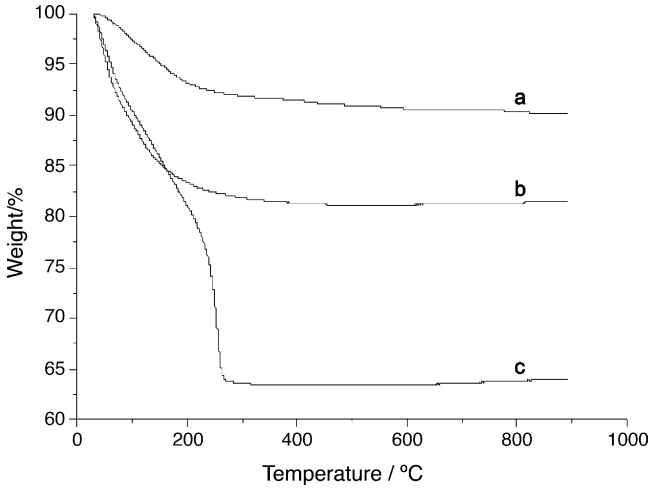

Fig. 1. Thermogravimetric analysis (wt.% vs. temperature) of (a) amorphous TiO_2–A2 after water washing, and of TiO_2–A1 after (b) and before (c) washing with water.

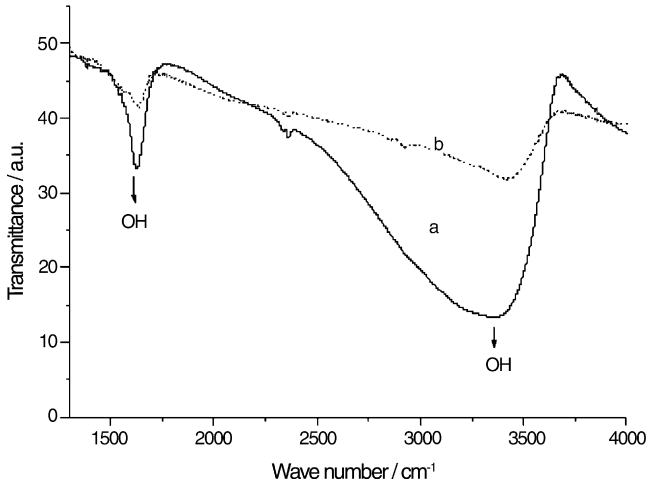

Fig. 2. The FT-IR spectra of (a) TiO_2–A1 and (b) TiO_2–A2. The O–H and Ti–O vibrations are labeled.

on the results obtained using ethanol as the solvent, as the data obtained from alternative solvents were closely similar. Prior to washing, the samples show a large weight loss of 38% owing to the presence of organic groups (ethanol/butanol), shown in Fig. 1. After washing, the TiO_2–A1 samples all exhibited a large ~19% weight loss (Fig. 1b) extending from 30 to 450 °C, corresponding to the formula $TiO_2 \cdot H_2O$ ($n = 1.04$). The weight loss of absorbed water in TiO_2–A2 was a lower 9.9%, and corresponded roughly to $TiO_2 \cdot 1/2H_2O$ ($n = 0.49$). Weight losses in this temperature range owe to the loss of surface water and hydroxyl groups, with the final product being the crystallization of TiO_2. Also, this weight loss remained reversible upon reimmersion in water until the temperatures at which the TiO_2 crystallizes (below). For example, approximately 52.2% of the original water content is removed by heating to 80 °C for 24 h, and this entire amount reabsorbed without any crystallization of anatase TiO_2 (see Supplementary Information). The FT-IR measurements, plotted in Fig. 2, show more intense O–H absorption peaks in TiO_2–A1 compared to that for TiO_2–A2, as expected from the larger amounts of absorbed water in $TiO_2 \cdot H_2O$ versus $TiO_2 \cdot 1/2H_2O$. The significance of high amounts of surface hydroxyl groups for the photocatalytic activity of amorphous ZrO_2 has been cited previously [18].

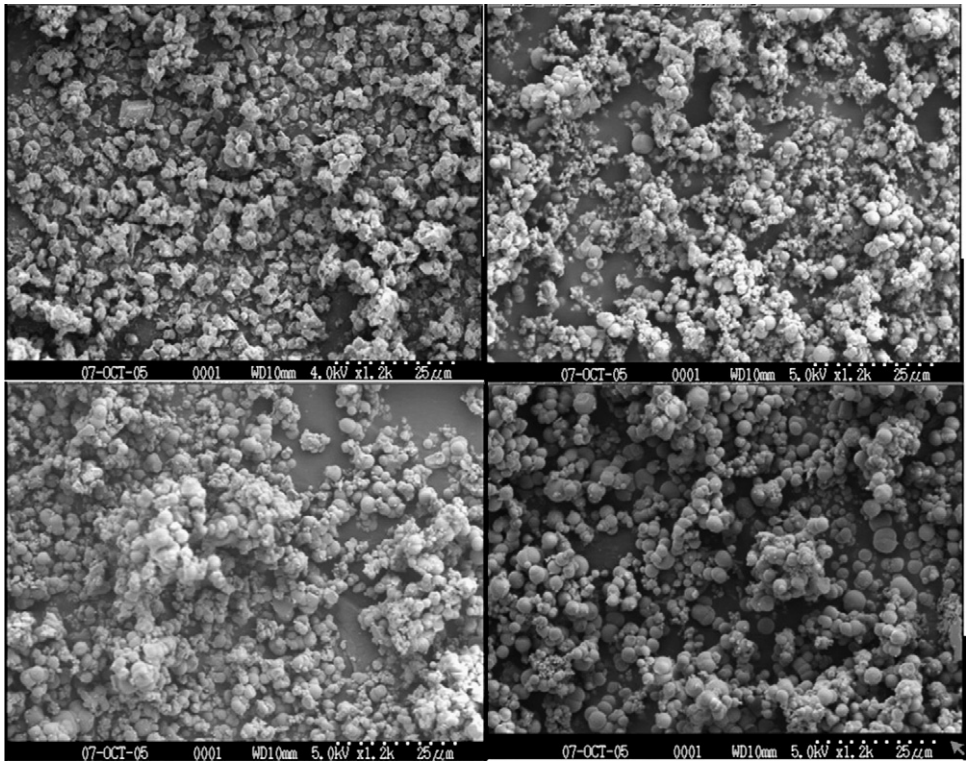

Fig. 3. SEM images of TiO_2–A1 prepared by dissolving Ti(*n*-butoxide)$_4$ in 2 ml (upper left), 5 ml (lower left), 10 ml (upper right), and 20 ml (lower right) ethanol.

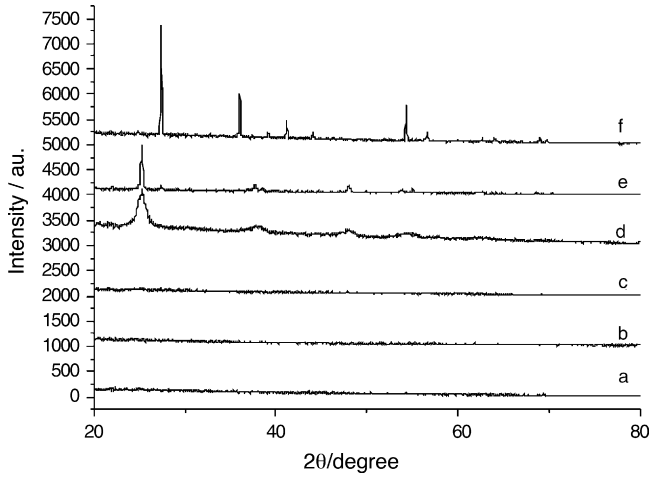

Fig. 4. Powder X-ray diffraction patterns for (a) synthesized TiO_2–A1, (b) after photocatalytic reaction, and calcined at temperatures of (c) 300 °C, (d) 400 °C, (e) 700 °C, and (f) 1000 °C.

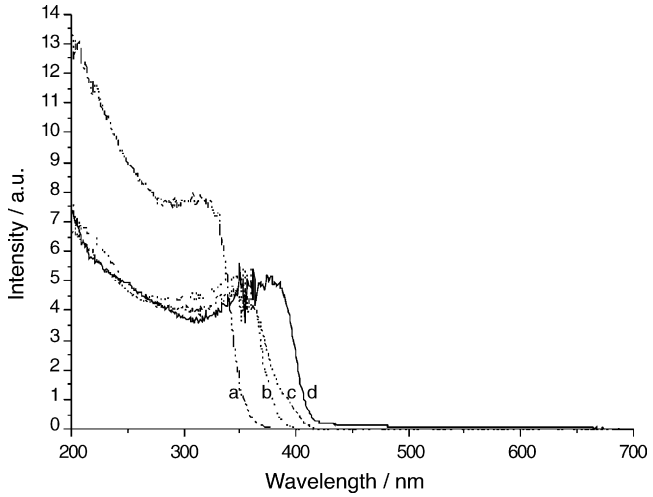

Fig. 5. The UV–vis diffuse reflectance spectra of (a) TiO_2–A1 and for the products calcined at (b) 400 °C, (c) 700 °C, and (d) 1000 °C.

Shown in Fig. 3, SEM analyses of TiO_2–A1 reveal increasing particle sizes and aggregation for increasing amounts of ethanol used in the preparation step. The larger particles result from the increased time for ethanol evaporation, but the different sizes do not effect the total amount of absorbed water found after washing with water. These particles are amorphous in nature and disperse into ultrafine particles upon washing with water.

Powder X-ray diffraction (PXRD) data were taken on TiO_2–A1 and also after its calcination at increasing temperatures of 100–1000 °C, shown in Fig. 4. No significant diffraction was detected in the samples prepared at 25 °C or dried at 80 °C, confirming the expected amorphous character of these solids. Each also remained amorphous after loading with 0.5–5.0 wt.% surface Pt and after photocatalytic reactions for >24 h (Fig. 4b). The PXRD of the TiO_2–A1 samples calcined at 300 °C also remained nearly featureless, but which exhibit a very weak emergence of diffraction peaks corresponding to crystalline anatase. Broad diffraction peaks for the anatase structure type appear at 400 °C and correspond to crystallite sizes of ~9.3 nm, as calculated from the Debye–Scherrer equation [23]. Previous reports of the synthesis of nanocrystalline TiO_2 are consistent with these results [14]. At the higher temperatures of 700 and 1000 °C, shown in Fig. 4e and f, the PXRD patterns correspond to a mixture of anatase and rutile or of rutile alone, respectively. Thus, TiO_2–A1 follows the expected transformation from amorphous to anatase to rutile forms of TiO_2 with increasing temperatures.

5.2. Optical properties and photocatalytic measurements

Optical band gaps of the TiO_2–A1 and TiO_2–A2 samples were calculated from their UV–vis diffuse reflectance spectra, shown in Fig. 5. The TiO_2–A1 samples have a band gap of ~3.4 eV, and which is slightly smaller than that of TiO_2–A2 at ~3.5 eV (see Supplementary Information). The onset of the absorption-edge for the samples calcined at 80, 400, 700, and 1000 °C was 352.6 nm (band gap = 3.5 eV), 374.8 nm (3.31 eV), 392.9 nm (3.16 eV) and 410.4 nm (3.02 eV) respectively. Metal oxides typically show a decreased band-gap size with increasing particle size or with a change in phase, such as from amorphous to anatase to rutile [12]. The band gap sizes reach a maximum in the amorphous samples, and which likely leads to higher conduction band levels for the reduction of water. For example, larger crystals of anatase TiO_2 require *n*-type doping to be photocatalytically active, while the rutile form has the smallest band gap and is inactive. The nanocrystalline and amorphous hydrated forms TiO_2 therefore do not suffer from this limitation, and which makes high rates of H_2 evolution possible.

The photocatalytic activities of all samples were tested in aqueous (20%) methanol solutions under band gap illumination, wherein the photoexcited electrons function as the reductants of water to give H_2 and the sacrificial methanol reacts rapidly with the photoexcited holes at the surface to give CO_2. The net reaction is: $CH_3OH(aq) + H_2O(l) \rightarrow CO_2(g) + 3H_2(g)$. Photocatalytic reactions in aqueous methanol are used to measure the rate of H_2 formation without the concomitant four-electron oxidation of H_2O to O_2. The latter oxidation can be assisted by a RuO_2 surface cocatalyst [24]. Because the deposition of the RuO_2 cocatalyst requires high temperatures (>300 °C), which would crystallize the amorphous TiO_2, the current studies were limited to using sacrificial methanol and a Pt cocatalyst. Shown in Fig. 6 is H_2 evolution versus time for TiO_2–A1 with 0 wt.% (b) and 0.5 wt.% Pt cocatalyst (a). The amount of gas produced increased linearly in all samples in the TiO_2–A1 series (prepared from either ethanol, acetone, THF or hexane), with calculated rates of 1100–1200 $\mu mol\, h^{-1}\, g^{-1}$ using 0.5 wt.% Pt cocatalyst, and lower rates of 250–350 $\mu mol\, h^{-1}\, g^{-1}$ using no cocatalyst. The optimum amount of Pt cocatalyst was found to be 0.5 wt.%, shown in the inset of Fig. 6, and gave rates 3.3 times higher than similar samples with no cocatalyst. By comparison, the maximum photocatalytic rates for H_2 production of the TiO_2–A2 samples were a much lower 170 $\mu mol\, h^{-1}\, g^{-1}$ with no Pt cocatalyst, and only a moderately higher rate of 210 $\mu mol\, h^{-1}\, g^{-1}$ for 0.5 wt.% Pt. These rates are from half to five times less than in TiO_2–A1, and shows the Pt cocatalyst has little effect on its activity. Shown in Fig. 7, the photocatalytic activity of TiO_2 samples calcinated at 80–1000 °C shows a maximal rate at 400 °C

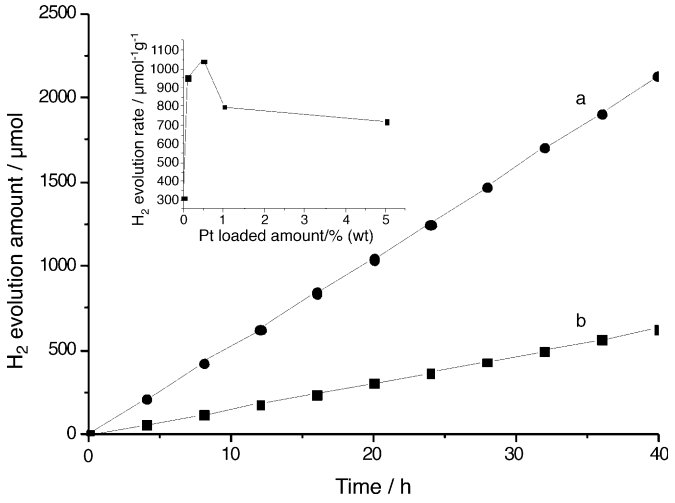

Fig. 6. Rate of H_2 production upon irradiation of TiO_2–A1 at 58 °C with 0.5% Pt cocatalyst (a) and no Pt cocatalyst (b). Inset: photocatalytic H_2 evolution rate vs. the amount of Pt loading.

that is ~5.7 times higher than amorphous hydrated TiO_2–A1, and is associated with the onset of crystallization of anatase. At 1000 °C negligible photocatalytic activity is observed, and is related to the conversion of anatase to rutile TiO_2. The photocatalytic rates for crystalline anatase increase by a factor of up to seventeen with the loading of 5 wt.% Pt cocatalyst [22]. The effect of the surface Pt sites on the resultant activity is smaller for amorphous TiO_2 than for anatase, and suggests either (a) a shortened mean free path of the excited electrons in the amorphous samples decreases their probability of reaching the Pt cocatalyst sites and/or (b) the mechanism of electron transfer across the hydrated interfaces of the amorphous samples utilizes a different pathway and therefore shows a less marked increase with Pt loading. The former seems more likely owing to the disordered nature of an amorphous solid.

The production of gas continues indefinitely under irradiation with a constant CO_2/H_2 ratio in the gas chromatographs (Supplementary Information), and clearly indicates the reactions

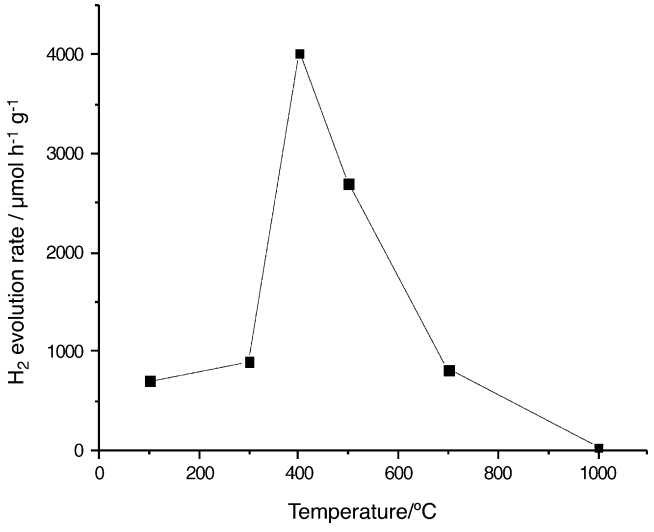

Fig. 7. Photocatalytic rates as a function of the calcination temperature of TiO_2–A1.

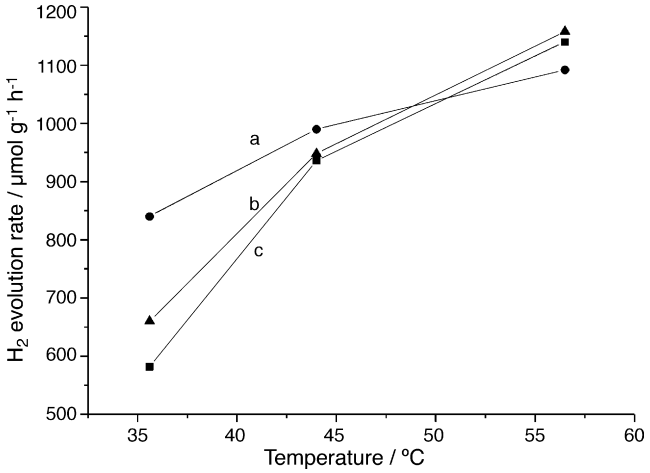

Fig. 8. The temperature dependence of the photocatalysis rates of TiO_2–A1 prepared from in hexane (a), acetone (b), and ethanol (c).

are photocatalytic. The total molar amount of H_2 generated by a continuous 40 h irradiation of TiO_2-A1 (ethanol), 629 μmol H_2 without Pt and 2,131 μmol H_2 with 0.5 wt.% Pt, exceeded the starting amount of TiO_2 of 626 μmol. The temperature dependence of the photocatalytic rates, plotted in Fig. 8 for 0.5 wt.% Pt cocatalyst, shows that when the reaction cell is kept at a lower 35 °C the rates decrease to ~550–850 μmol h^{-1} g^{-1}. The positive correlation of temperature with photocatalytic rates has been connected to the adsorption/desorption equilibria at the active sites of TiO_2, and as well, to the diffusion rates to and from the surface [25,26]. An optimal temperature range of 60–80 °C has been reported in related photocatalytic studies of crystalline TiO_2. Thus, lower temperatures have a dramatic and negative impact on the photocatalytic rates for amorphous hydrated TiO_2 as well. Because much photocatalysis research is performed using IR filters, unlike under real solar illumination, this suggests a significant possible discrepancy between rates measured in the lab and the rates that can possibly be obtained in applications.

5.3. Surface Ti^{3+} sites

Without a surface Pt cocatalyst, both TiO_2–A1 and TiO_2–A2 will turn blue-grayish upon illumination by band gap light owing to the formation of Ti^{3+} (an effect noted in crystalline TiO_2 as well). The formation of Ti^{3+} is associated with either slow electron transfer and/or the trapping of electrons at defect sites [12,23,27]. A higher concentration of Ti^{3+} should correspond to a larger number of available active sites on the surfaces, becoming trapped until the reaction with water at the surface to give H_2 and Ti^{4+} back again. When both samples of amorphous hydrated TiO_2 (–A1 and –A2) were irradiated for 20 min, without a Pt cocatalyst and in the absence of O_2, the absorption of visible light (i.e. Ti^{3+} sites) in the TiO_2–A1 sample was found to be larger than in the TiO_2–A2 sample. These results are consistent with the higher photocatalytic rates for the former. However, previous studies on other amorphous TiO_2 samples have correlated the large buildup of Ti^{3+} concentration with negligible photocatalytic activity [14]. The effect cited therein is an increased probability of electron–hole recombination at the

defect sites. However, the presence of abundant surface water and reactive methanol species for the TiO_2–A1 and –A2 samples must help to substantially suppress the recombination of holes with the electrons at the Ti^{3+} sites. The larger amounts of absorbed water for TiO_2–A1 ($TiO_2{\cdot}H_2O$) compared to TiO_2–A2 ($TiO_2{\cdot}1/2H_2O$), and therefore higher reactive surface area, should be noted as a significant factor in promoting the greater concentration of Ti^{3+} and higher photocatalytic rates for H_2 evolution.

6. Conclusions

The hydrated forms of amorphous titania, $TiO_2{\cdot}nH_2O$, can be prepared at room temperature and exhibit significant photocatalytic rates in aqueous methanol solutions. All samples exhibited slightly larger band gap sizes than that of nanocrystalline anatase, at ~3.4–3.5 eV. For platinized samples the photocatalytic rates varied from a low of 210 $\mu mol\,h^{-1}\,g^{-1}$ up to a maximum measured rate of 1158 $\mu mol\,h^{-1}\,g^{-1}$. The photocatalysis rates did not vary with the type of solvent used in the preparation, involving either ethanol, acetone, hexane or tetrahydrofuran. However, elevated temperatures of just ~58 °C resulted in up to a two-fold increase in their photocatalytic rates. The high photocatalytic rates for the hydrated forms of amorphous TiO_2 are associated with the larger amounts of absorbed surface water and methanol species at the active sites, as revealed in the higher concentrations of Ti^{3+} at the surfaces upon band gap illumination.

Acknowledgment

The authors acknowledge support of this work from the Beckman Foundation in the form of a Beckman Young Investigator Award (P.M.).

Appendix A. Supplementary data

Supplementary data associated with this article can be found, in the online version, at doi:10.1016/j.jphotochem.2006.07.004.

References

[1] M. Grätzel (Ed.), Energy Resources through Photochemistry and Catalysis, Academic Press, New York, 1983.
[2] K. Yamaguti, S. Sato, J. Chem. Soc. Faraday Trans. I 81 (1985) 1237.
[3] K. Sayama, H. Arakawa, J. Phys. Chem. 97 (1993) 531.
[4] K. Sayama, H. Arakawa, J. Photochem. Photobiol. A 77 (1994) 243.
[5] J.M. Lehn, J.P. Sauvage, R. Ziessel, L. Hilaire, Israel J. Chem. 22 (1982) 168.
[6] H. Kato, A. Kudo, Catal. Lett. 58 (1999) 153.
[7] J.R. Darwent, A. Mills, J. Chem. Soc. Faraday Trans. 278 (1982) 359.
[8] O. Carp, C.L. Huisman, A. Reller, Prog. Solid State Chem. 32 (2004) 33.
[9] M.R. Hoffmann, S.T. Martin, W.Y. Choi, D.W. Bahnemannt, Chem. Rev. 95 (1995) 69.
[10] X.F. You, F. Chen, J.L. Zhang, J. Sol–Gel Sci. Technol. 34 (2005) 181.
[11] Y. Oosawa, M.J. Grätzel, Chem. Soc., Faraday Trans. 1 84 (1988) 197.
[12] R.S. Davidson, C.L. Morrison, J. Abraham, J. Photochem. 24 (1984) 27.
[13] K. Tanaka, M.F.V. Capule, T. Hisanaga, Chem. Phys. Lett. 187 (1991) 73.
[14] B. Ohtani, Y. Ogawa, S.I. Nishimoto, J. Phys. Chem. B 101 (1997) 3746.
[15] H. Jensen, K.D. Joensen, J.-E. Jørgensen, J.S. Pedersen, E.G. Søgaard, J. Nanopart. Res. 6 (2004) 519.
[16] A. Kudo, A. Tanaka, K. Domen, K. Maruya, K. Aika, T. Ohnishi, J. Catal. 111 (1988) 67.
[17] T. Takata, K. Shinohara, A. Tanaka, M. Hara, J.N. Kondo, K. Domen, J. Photochem. Photobiol. 106 (1997) 45.
[18] H. Kominami, K. Oki, M. Kohno, S.I. Onoue, Y. Kera, B. Ohtani, J. Mater. Chem. 11 (2001) 604.
[19] C.Y. Wu, X.P. Zhao, Y.J. Ren, Y.H. Yue, W.M. Hua, Y. Cao, Y. Tang, Z. Gao, J. Mol. Catal. A: Chem. 229 (2005) 233.
[20] M.K.I. Senevirathna, P.K.D.D.P. Pitigala, K. Tennakone, J. Photochem. Photobiol. A: Chem. 171 (2005) 257.
[21] C.Y. Hsiao, C.L. Lee, D.F. Ollis, J. Catal. 82 (1983) 418.
[22] T. Kawai, T. Sakata, J. Chem. Soc. Chem. Commun. 15 (1980) 694.
[23] H. Klug, L.E. Alexander, X-ray Diffraction Procedures, 2nd ed, John Wiley and Sons, Inc., New York, 1974.
[24] T. Kawai, T. Sakata, Chem. Phys. Lett. 72 (1980) 87.
[25] J.-M. Herrmann, Top. Catal. 34 (2005) 49.
[26] S. Yamazaki, S. Tanaka, H. Tsukamoto, J. Photochem. Photobiol. A: Chem. 121 (1999) 55.
[27] D. Duonghong, J. Ramsden, M. Grätzel, J. Am. Chem. Soc. 104 (1982) 2977.